Thin-Walled Structures 107 (2016) 543–553

Contents lists available at ScienceDirect

Thin-Walled Structures

journal homepage: www.elsevier.com/locate/tws

Full length article

Optimum crashworthiness design of tapered thin-walled tubes with lateral circular cutouts

A. Taştan, E. Acar, M.A. Güler*, Ü. Kılınçkaya

Department of Mechanical Engineering, TOBB University of Economics and Technology, Söğütözü, Ankara 06560, Turkey

ARTICLE INFO

Article history:
Received 22 December 2015
Received in revised form
22 July 2016
Accepted 22 July 2016
Available online 25 August 2016

Keywords:
Crush force efficiency
Specific energy absorption
Finite element analysis
LS-DYNA
Surrogate models
Multi-objective optimization
Circular cutouts
Thin-walled tubes

ABSTRACT

In this paper, the effects of introducing lateral circular cutouts on crash performances of tapered thin-walled tubes are explored within a simulation-driven surrogate-based multi-objective optimization framework. The crash performances of the tubes are measured using the crush force efficiency (CFE) and the specific energy absorption (SEA) criteria, which are computed using the finite element analysis code LS-DYNA. Surrogate-based optimization approach is followed to find out that optimum values of the wall thickness, the taper angle, the cutout diameter and the numbers of cutouts in horizontal and vertical directions to maximize CFE and SEA. Four different surrogate models are used: polynomial response surfaces, radial basis functions, and Kriging models with zeroth- and first-order trend models. It is found that the optimum CFE of the tubes with lateral circular cutouts is 27.4% larger than the optimum CFE of the tubes without cutouts. It is also found that the optimum SEA of the tubes with lateral circular cutouts is 26.4% larger than the optimum SEA of the tubes without cutouts. It is observed that the optimum SEA design has slightly reduced wall thickness, significantly reduced taper angle, significantly increased cutout diameter, increased number of cutouts in horizontal direction and slightly reduced number of cutouts in vertical direction compared to the optimum CFE design. In addition, multi-objective optimization of the tubes is performed by maximizing a composite objective function that provides a compromise between CFE and SEA. It is found that the CFE dominates the behavior of composite objective function.

1. Introduction

In recent years, thin-walled structures have been increasingly used as crash absorbers which convert impact energy into internal energy through structural deformation. Tubular structures are the most common type due to their simple, efficient shape and also ease of manufacture and assembly in the industry. The main goal of these crash absorbers is to transfer minimum amount of crash energy to the occupants and the main parts of the vehicle in case of a collision. In a crash incident, crash absorber is deformed plastically and a great part of energy is absorbed during the collision. It becomes unusable (i.e., discarded) after a single crush. Light-weight design of these crushable parts are still studied by many researchers in order to have excellent crashworthiness and formability.

To predict and observe the crushing behavior of thin-walled tubes under axial impact loading, there have been numerous researches in the literature. These studies have mainly focused on circular [1–4] and square [1,5] types of tubes, while many different types of cross-sectional shapes exist such as hexagonal [1,6] or octagonal [7]. Tubular structures have a wide range of options including straight and tapered types. All side-walls are parallel to the longitudinal axis of the tube in the straight types. However, for tapered types, at least one side-wall is oblique with respect to the longitudinal axis. Tapered crash absorbers are more advantageous to the straight tubes since they are effective for both oblique and axial impact loads [8]. Energy absorption capability of different tapered tubes under axial impact loading was investigated by Nagel and Thambiratnam [9]. They varied the number of tapered sides and the wall thickness. Liu [10] performed a design optimization for the tapered tubes with square sections, where section's side length, wall thickness and tapering angle are design variables. Paralleling the strategy in tapering the tubes, there are many other suggestions which propose reducing the initial peak load or increasing the amount of absorbed energy. Applying imperfections and geometrical discontinuities, such as grooves [11], cutouts (or holes) [12,13], dents [14] and corrugations [1,15,16], is the prevalent one. In addition to these conventional modification methods, some studies propose a topological change of the tube sidewalls including the form of circular cutouts [17] or rectangular

* Corresponding author.
E-mail address: mguler@etu.edu.tr (M.A. Güler).

http://dx.doi.org/10.1016/j.tws.2016.07.018
0263-8231/

windows [18]. The energy absorption characteristics of the tubes with laterally drilled cutouts under axial impact loading were investigated by Arnold and Altenhof [19]. They experimentally observed the effect of location and diameter of the cutouts on the energy absorption behavior. For the square form of cutouts, Han et al. [20] studied crushing behavior under axial loading by changing the location of cutout and tube length. Also, Bodlani et al. [21] varied number of cutouts and cutout diameters with different cutout spacing configurations for square tubes. Common among the aforementioned studies is to investigate the effect of tapering or geometrical discontinuities in the form of cutouts only. This paper aims to analyze both the effect of tapering and geometrical discontinuities in the form of cutouts.

During the axial crushing process of thin-walled tubes, crushing forces are generated to overcome the resistance of the tube. For a crashworthy energy absorber design, the tubes under axial impact loading are expected to provide both high energy absorption and stable reaction force. In other words, they should have a fairly uniform response to impact load after the initial peak. At the start of axial crushing process, initial peak force should be as low as possible to minimize the injury and damage, while the ability of energy absorption of the tube is being improved. Accordingly, both peak crush force and energy absorption values should be taken into consideration in determining the optimal design of a crush absorber. One of the common way to determine the optimal design is the calculation of crush force efficiency (CFE) and specific energy absorption (SEA). CFE and SEA can be described as the ratio of mean crush force to the peak crush force and the energy absorption per unit mass, respectively. For example, Arnold and Altenhof [19] studied the effect of circular cutouts centrally located into the two opposing walls of the square tubes by comparing the CFE and SEA values. Han et al. [20] characterized the crushing behavior of tubes with a cutout by evaluation of SEA values. On the other hand, weight of the structure is another remarkable factor for a commercial design. Song et al. [18] aimed to reduce weight by introducing patterned windows to the thin-walled square tubes. They performed a parametric study in terms of SEA. SEA parameter do not only provide a great information about the efficiency of crash absorber but also it may lead to a light-weight design of energy absorbing component, which the weight and the material cost of the structure are also crucial.

The main objective of this study is to analyze tapered tubes with geometrical discontinuities in the form of lateral circular cutouts, where the wall thickness, the tapering angle, the cutout diameter, and the numbers of cutouts in horizontal and vertical directions are considered as design variables. Such an analysis can be conducted using either experimental or numerical methods (e.g., finite element method (FEM)). Since experiments are expensive and time demanding, and FEM has become a widely accepted technique in engineering applications, FEM is used in this paper to analyze several designs without the need of building an testing them. The commercially available explicit dynamic finite element (FE) analysis code LS-DYNA [22] is used in this study to simulate the crash behavior of thin-walled tubes under axial impact loading. The simulations of the thin-walled tubes are performed based on the loading conditions in a standard high-speed crash test, European New Car Assessment Program (Euro NCAP) [23].

In this study, the global geometrical properties (the wall thickness and the taper angle) as well as the local geometrical properties (the cutout diameter and the numbers of cutouts in horizontal and vertical directions) are optimized to maximize the CFE and the SEA. The main challenge in solving this optimization problem is related to the very large computational costs of performing FE simulations, and the use of surrogate models is a common and practical approach. Several researchers performed structural optimization of the vehicles or their components by using surrogate models (e.g., [24–30]). In particular, some researchers focused on energy absorption capabilities of the thin-walled tubes, and used surrogate models to perform crashworthiness optimization of these tubes [10,31–36]. In this study, multi-objective surrogate-based optimization of the tubes are performed to determine the global and local geometrical properties of tapered thin-walled tubes with lateral circular cutouts for maximum CFE and SEA.

The remainder of the paper is organized as follows: The next section provides the description of the optimization problem. Section 3 presents the details of the finite element analysis of the tapered thin-walled tubes with lateral circular cutouts. Section 4 discusses the construction and accuracy evaluation of the surrogate models. Section 5 presents and discusses the results of the optimization problem. Finally, the concluding remarks are given in Section 6.

2. Problem description

Differently from previous conventional modification methods [14–16], the thin-walled tubes having circular cross sections have

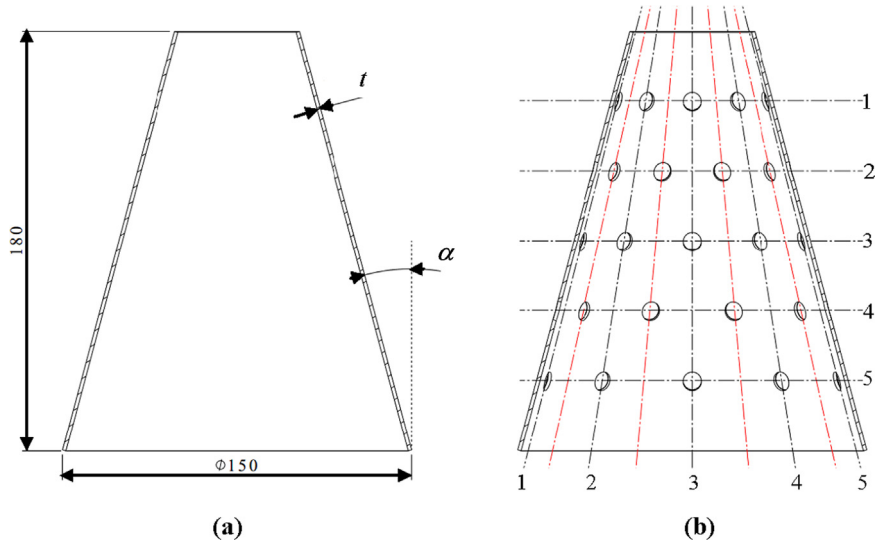

Fig. 1. The geometry of the thin-walled tube (a) without, and (b) with circular cutouts. *The dimensions are in millimeters.*

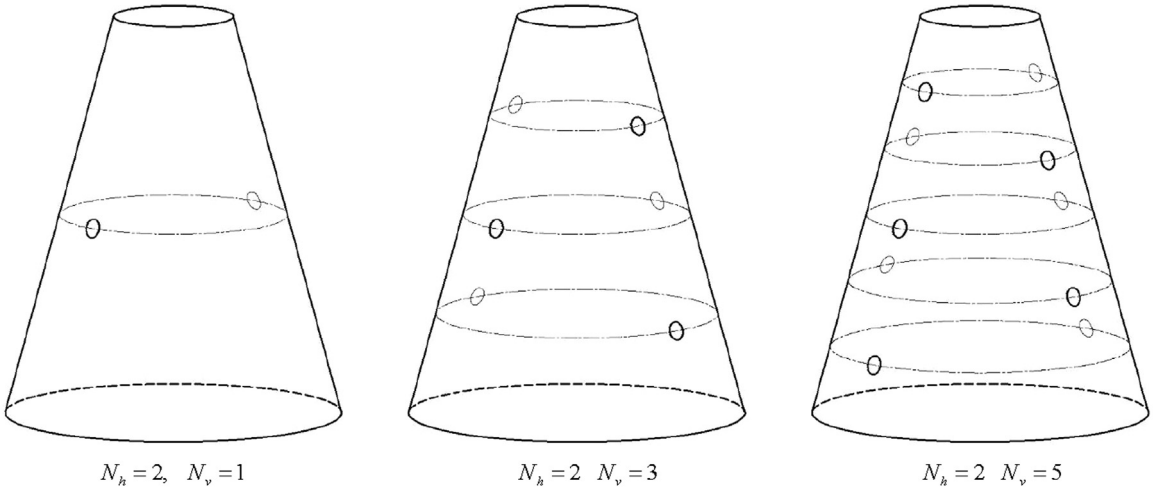

Fig. 2. The geometry of the thin-walled tube with circular cutouts.

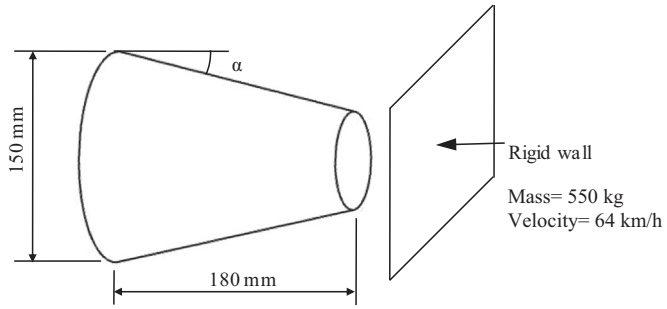

Fig. 3. The tube impacted with a rigid wall.

been modeled with and without geometrical discontinuities in the form of circular cutouts as shown in Fig. 1. The application of lateral circular cutouts to the side-walls of the tubes can alternatively be called as a topological pattern design, which is explicitly illustrated in Fig. 2. The tubes have a largest diameter of 150 mm, and a length of 180 mm. For the crash performance of tubes, the following design problem is considered. The aim is to achieve both crashworthy and light-weight design. The tubes are impacted with a 550 kg rigid wall with an initial velocity of 64 km/h (see Fig. 3) corresponding to standard high-speed crash test of Euro NCAP.

The crash performance of the tubes is evaluated by two metrics: CFE and SEA. In optimization, these two metrics are selected as objective functions. The design variables are chosen as (i) the tube wall thickness (t), (ii) the taper angle (α), (iii) the diameter of circular cutouts (d), (iv) the number of cutouts in horizontal direction (N_h), and (v) the number of cutouts in vertical directions (N_v). Therefore, the optimization problem for maximum CFE (or maximum SEA) can be stated as

$$\begin{aligned} &\text{Find} && t,\ \alpha,\ d,\ N_h,\ N_v \\ &\text{Min} && -CFE\ (\text{or } -SEA) \\ &\text{Such that} && 2\ \text{mm} \le t \le 3.5\ \text{mm} \\ & && 0 \le \alpha \le 15^\circ \\ & && 5\ \text{mm} \le d \le 15\ \text{mm} \\ & && 2 \le N_h \le 10 \\ & && 1 \le N_v \le 5 \end{aligned} \tag{1}$$

In this study, the effect of the use of the lateral circular cutouts are evaluated by comparing the energy absorption capacity of the thin-walled tubes with lateral circular cutouts to those of the thin-walled tubes without cutouts. Therefore, a separate optimization problem is formulated for the tubes without cutouts as follows:

$$\begin{aligned} &\text{Find} && t,\ \alpha \\ &\text{Min} && -CFE\ (\text{or } -SEA) \\ &\text{Such that} && 1\ \text{mm} \le t \le 2.5\ \text{mm} \\ & && 0 \le \alpha \le 15^\circ \end{aligned} \tag{2}$$

Notice that the optimization problem stated in Eq. (2) is a two-variable optimization problem, and the bounds of the wall thickness is changed to [1, 2.5] mm (compared to [2, 3.5] mm in Eq. (1)) in order to obtain similar weights for the tubes with and without cutouts. The bounds of the taper angle, on the other hand, is kept unchanged.

In addition to formulating a single-objective optimization problem to maximize either for CFE or SEA, a multi-objective optimization problem is also formulated by defining a composite objective function that can provide a compromise between CFE and SEA. The composite objective function that will be maximized is defined as

$$F = w\frac{CFE}{CFE_0} + (1-w)\frac{SEA}{SEA_0} \tag{3}$$

where F is the composite objective function, w is a weight factor that specifies the relative importance CFE and SEA, and CFE_0 and SEA_0 are the normalization constants for the CFE and SEA, respectively. Here, the values of these normalization constants are taken as the maximum CFE and SEA values obtained at the training points.

The optimization problems defined in this section are solved by using "*fmincon*" built-in function of MATLAB [37] based on sequential quadratic programming. To increase the chance of finding the global optimum, the optimization runs used 100 different randomly selected starting points. The optimization results in real numbers for the numbers of cutouts in horizontal and vertical directions, even though these design variables should have integer numbers. To resolve this issue, the following approach is followed. After the optimum solution is obtained as real numbers for these design variables, the nearest two integers are considered for each design variable, hence four combinations are considered. For instance, if the optimum values are found to be N_h=8.83 and N_v=2.36, then the following four (N_h, N_v) combinations are considered: (8, 2), (9, 2), (8, 3), and (9, 3). For each of these four combinations, the optimization problem in Eq. (1) is reduced to a three-variable optimization problem (in terms of t, α and d only),

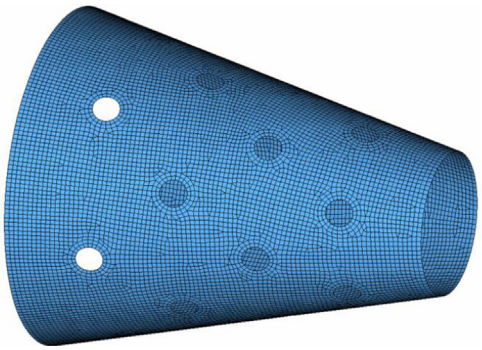

Fig. 4. Finite element mesh of the tube with lateral circular cutouts.

and the optimum values of N_h and N_v are calculated. Finally, the combination with the best performance (i.e., the minimum objective function value) is declared as the optimum.

3. Finite element simulations

The collapse behavior of the tubes has been simulated by using explicit, nonlinear finite element code LS-DYNA. The finite element models of the tubes are created by using the commercial preprocessor software HYPERMESH [38]. Thin-walled tubes were fixed at one end and impacted by a rigid wall having an initial velocity of 64 km/h and a mass of 550 kg in axial direction.

Belytschko-Lin-Tsay shell elements having five integration points through the thickness were employed to model thin-walled tubes having circular cross sections. The side-walls of the tube profiles have both tapering angle and circular cutout patterns as shown in Fig. 1b. Thus, the numerical model consists of mostly quadrilateral elements and small number of triangular elements (less than % 2) due to the existence of curvatures on the tube surfaces. The target size of these elements is chosen to be 2 mm, based on a mesh convergence study. To observe the accurate effect of topological pattern design, double washers are added around the circular cutouts by using quadrilateral elements of 1.8 mm element size. The schematic of the finite element mesh with lateral circular cutouts is shown in Fig. 4.

The material models used in the Finite Element model are the "*Material type 20 rigid material*" for the rigid wall and the "*Material type 24 elasto-plastic material*" for the tube. For Material type 24, the plastic region is included with true stress-true strain curve. Mild steel properties are used for the tubes. Material properties are taken from an earlier work (Acar et al. [2]) and given in Table 1. Also, the validation of the FE models is provided in [2].

For contact definitions, "automatic single surface" contact algorithm is used. The self-contact of the tubes, and the contact between the tube and the rigid wall are defined by using this type of contact. The friction coefficients used in Ref. [2] are employed in this study. That is, the static and dynamic friction coefficients for the tubes are taken as 0.3 and 0.2, respectively. The friction coefficient between the tube and the moving rigid wall is taken to be 0.3.

Table 1
True stress-true plastic strain values for mild steel.

σ_t [MPa]	331	347	390	427	450	469	501	524	533	533
ε_p	0	0.018	0.0374	0.056	0.075	0.093	0.138	0.18	0.23	0.5

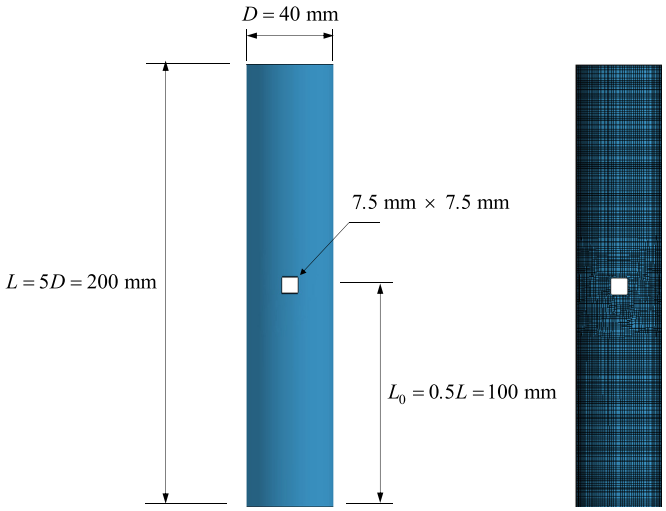

Fig. 5. Geometry and the finite element model used in the validation study.

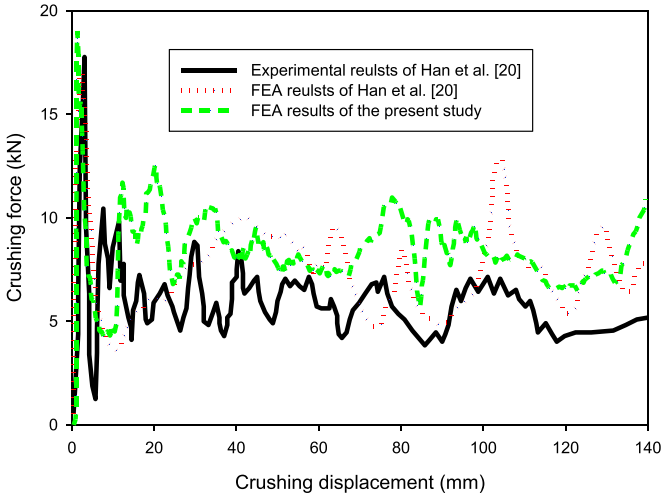

Fig. 6. Comparison of the force-displacement curve obtained from the finite element model of the present study to the force-displacement curves obtained from the experimental and the finite element results of Han et al. [20].

4. Validation of the finite element model

The finite element model used in crash simulations are validated by using the experimental results of Han et al. [20], where crushing tests were conducted on aluminum tubes of intermediate length (L=5D=200 mm, where L and D denote the length and the diameter of the tube, respectively). Han et al. [20] drilled square cutouts at three different locations L_0=0.50L, L_0=0.75L, and L_0=0.95L, and they performed both quasi-static tests (crushing speed of 10 mm/min) and dynamic impact tests (impact speed varying from 6 m/s to 20 m/s). In the present paper, we used the experimental results corresponding to the following case: the cutout was located at the mid-length (that is, L_0=0.50L), and impact speed of 6 m/s was used (see Fig. 5). For validation of our finite element model, the force-displacement curves as well as the deformation modes are used.

The force-displacement curve obtained from the finite element model of the present study are compared to the force-displacement curves obtained from the experimental and the finite element results of Han et al. [20] in Fig. 6. It is found that the results of the finite element model of the present study are good agreement with the experimental and the finite element results of Han et al. [20].

Table 2
Comparison of the absorbed energy, the peak crushing force, the specific energy absorption, and the mean crushing force values obtained from to the finite element model of the present study to those obtained from Han et al. [20].

	Absorbed energy (J) @28.3 ms	Peak crushing force (kN)	SEA (J/kg)	Mean crushing force (kN)
A) **Experimental results (Han et al. [20])**	811.2	17.80	13,446.9	5.79
B) **Finite element results (Han et al. [20])**	1050.0	17.13	17,405.4	7.46
C) **Finite element results of the present study**	1093.1	18.28	18,119.9	8.11
% Difference between B and A	29.4	−3.8	29.4	28.8
% Difference between C and A	34.8	2.7	34.8	40.0

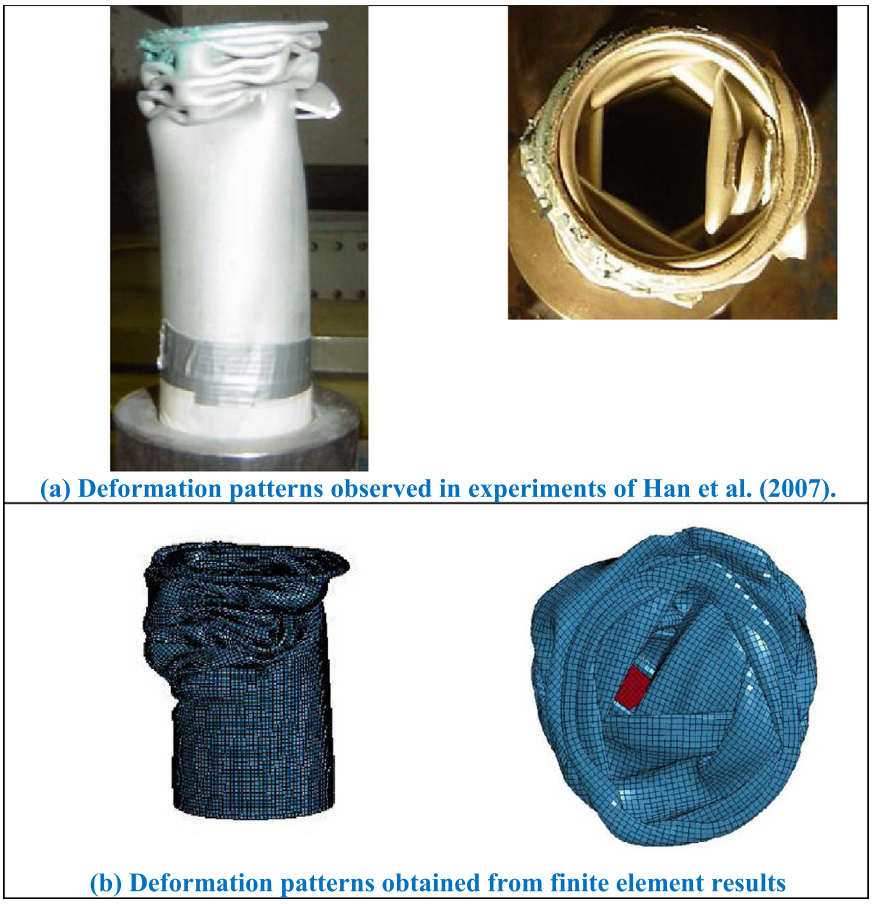

Fig. 7. Comparison of the deformation patterns obtained from the finite element model of the present study to the ones observed in experiments.

Furthermore, the force-displacement curve corresponding to the experimental results as well as the finite element results of Han et al. [20] are also used to compute the four widely-used responses in a crush scenario: the absorbed energy, the peak crushing force, the specific energy absorption, and the mean crushing force. These values are compared to the finite element results of the present study and provided in Table 2. It is found that the finite element predictions of the current study and the finite element predictions of Han et al. [20] have similar errors.

Finally, the deformation patterns obtained from the finite element model of the present study are compared to the deformation patterns observed in experiments of Han et al. [20]. Fig. 7 shows good agreement in deformation patterns.

5. Surrogate models

In simulation based design optimization, if the simulations are computationally very expensive, then the use of surrogate models is a common and practical approach. A surrogate model is an approximation model that can mimic the behavior of a complex simulation model as closely as possible while being computationally more efficient to evaluate. A surrogate model is constructed based on the response data at some specified training points that are selected by using a proper design of experiments (DOE) techniques within the bounds of the input variables. After the responses at the training points are evaluated, the matrix of input and output values are used to generate a surrogate model. Next, the accuracy of the generated surrogate model is evaluated. If the accuracy is found to be satisfactory, the surrogate model is used in optimization. If the accuracy is found to be unsatisfactory, then proper measures are taken to improve accuracy to an acceptable level.

5.1. Design of experiments

The first step of constructing a surrogate model is selecting a proper DOE type. Two main families of design of experiments exist [39]: (i) classic designs and (ii) space filling designs. The most commonly used classic experimental designs include fractional

Table 3
Training points and corresponding responses. *The maximum CFE, SEA and F (composite objective function) values obtained at the training points are depicted in bold fonts.*

No.	t (mm)	α (deg.)	CFE	SEA (kJ/kg)	F (for w=0.5)
1	1.712	10.727	0.4691	16.62	0.7333
2	1.662	0.401	0.3591	16.44	0.6478
3	2.301	1.078	0.4083	20.37	0.7756
4	1.063	6.213	0.3451	12.70	0.5505
5	2.088	4.752	0.4746	19.20	0.7973
6	1.994	12.129	0.5476	18.55	0.8362
7	1.769	7.910	0.4486	16.96	0.7262
8	1.185	8.550	0.3726	13.27	0.5842
9	2.230	13.531	**0.6767**	**21.49**	**1.0000**
10	1.880	3.699	0.4525	18.30	0.7600
11	2.377	4.070	0.4669	21.32	0.8411
12	2.438	11.268	0.5959	21.25	0.9347
13	1.262	13.265	0.4385	13.36	0.6348
14	1.598	14.748	0.5585	15.84	0.7812
15	2.136	9.108	0.5184	19.43	0.8351
16	1.969	6.894	0.4772	18.44	0.7817
17	1.355	5.788	0.3829	14.53	0.6209
18	1.476	10.158	0.4391	15.73	0.6905
19	1.416	2.858	0.3876	15.18	0.6396
20	1.135	1.993	0.3473	13.46	0.5697

factorial design (FFD), central composite design (CCD) and Box-Behnken designs [39]. Popular space filling designs include Latin hypercube sampling (LHS) designs [40], maximum entropy designs [41], minimax and maximin designs [42], and orthogonal arrays [43]. In this study, LHS design of experiments is used. The number of training points is selected to be ten times the number of variables (the rule of thumb). Therefore, 20 training points are used to generate the surrogate models for the tubes without cutouts, whereas 50 training points are used to generate the surrogate models for the tubes with lateral circular cutouts. The training points generated for the tubes without cutouts are the corresponding response values are given in Table 3. The training points generated for the tubes with cutouts are not given due to space limitations.

5.2. Construction of surrogate models

After the DOE type is selected, the locations of the training points are determined within the bounds of the design variables. Then, the CFE and SEA values at the training points are computed using LS-DYNA. Next, different types of surrogate models are constructed using the DoE information and the computed CFE and SEA values. Quadratic polynomial response surface (PRS) approximations, radial basis functions (RBF) and Kriging models with zeroth- and first-order trend models (KR0 and KR1), respectively, used as different types of surrogate models. A brief overview of the mathematical formulation of PRS, RBF KR0 and KR1 can be found in Appendix B of Acar et al. [2].

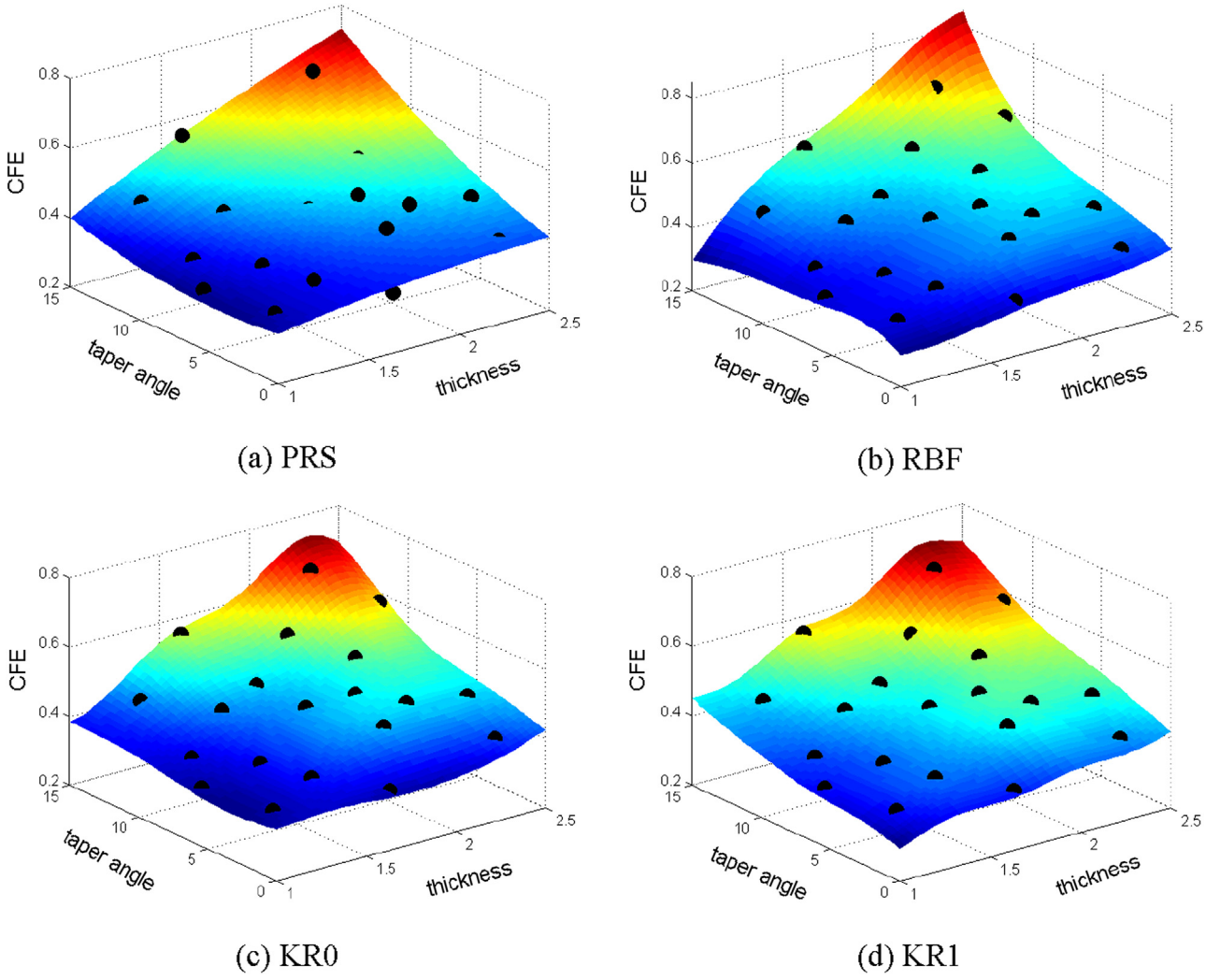

Fig. 8. Constructed surrogate models for CFE prediction. *The bold black dots in the plots show the training points.*

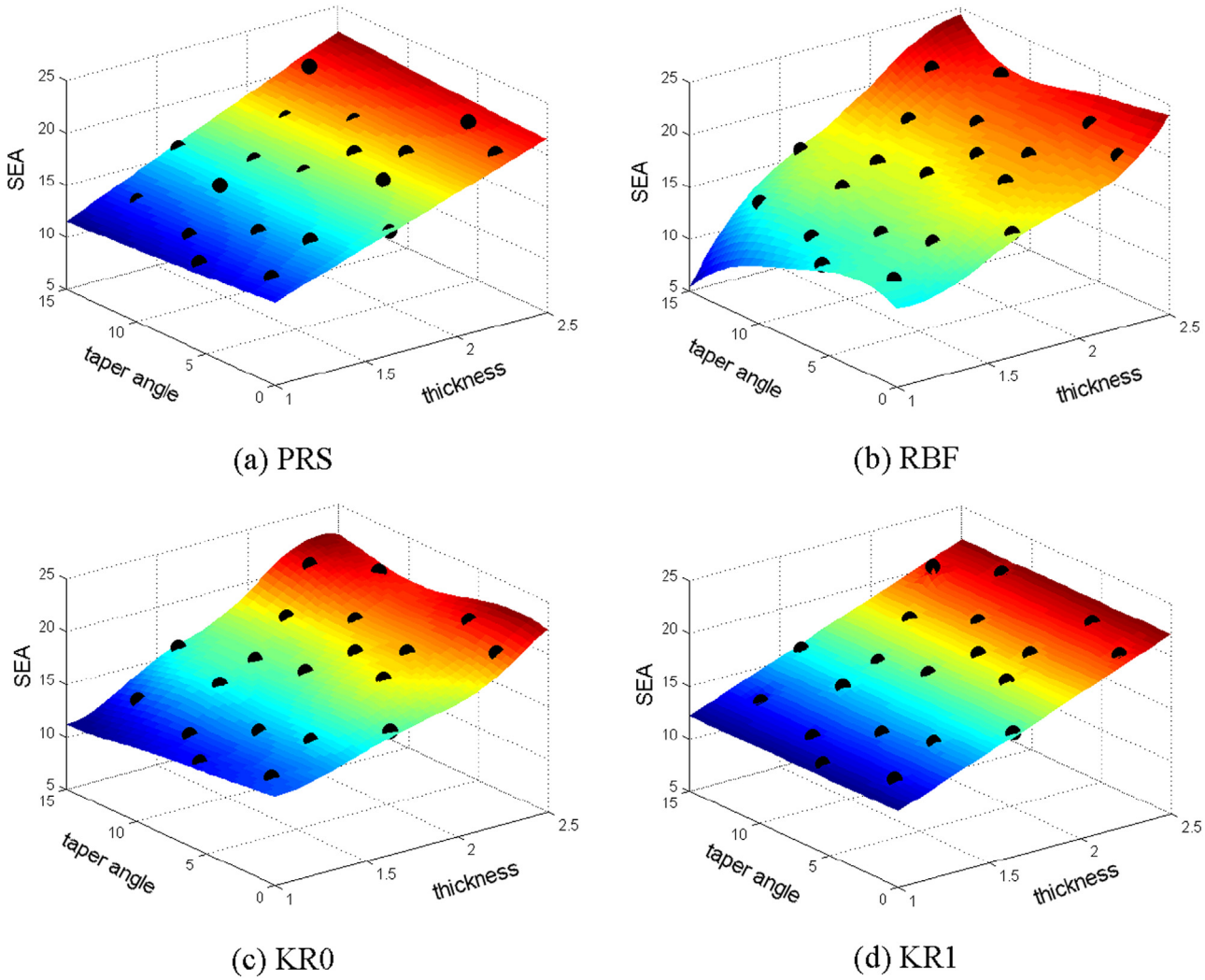

Fig. 9. Constructed surrogate models for SEA prediction. *The bold black dots in the plots show the training points.*

The constructed surrogate models for CFE prediction of the tubes without cutouts are shown in Fig. 8, and the surrogate models for SEA prediction of the tubes without cutouts are shown in Fig. 9. Notice that RBF, KR0 and KR1 surrogate models pass through all training points, while PRS2 does not. The surrogate models generated for CFE and SEA predictions of the tubes with lateral circular cutouts are not shown as the number of variables is five.

5.3. Accuracies of the constructed surrogate models

The accuracies of the constructed surrogate models are evaluated based on normalized version of the leave-one-out generalized mean square cross validation error (*GMSE*). The normalized GMSE is calculated as follows. If there are N training points, a surrogate model type is constructed N times, each time leaving out one of the training points. Then, the difference between the exact value of the response y^k at the omitted training point $\boldsymbol{x}_k$ and the predicted value of the response using the surrogate model is calculated. Finally, the normalized *GMSE* is calculated from

$$GMSE_{nor} = \frac{\frac{1}{N}\sum_{k=1}^{N}\left(y^k - \hat{y}^{(k)}\right)^2}{y_{\max} - y_{\min}} \tag{4}$$

Table 4
Accuracies of different types of surrogate models constructed for CFE and SEA predictions for the tubes without cutouts. *The smallest error in each row is shown in bold for ease of comparison.*

	PRS2	RBF	KR0	KR1
Accuracies of surrogate models for CFE prediction				
Normalized generalized mean square cross validation errors (%)	7.8	**7.3**	10.1	8.9
Accuracies of surrogate models for SEA prediction				
Normalized generalized mean square cross validation errors (%)	6.1	8.2	8.8	**5.5**

Table 5
Accuracies of different types of surrogate models constructed for CFE and SEA predictions for the tubes with cutouts. *The smallest error in each row is shown in bold for ease of comparison.*

	PRS2	RBF	KR0	KR1
Accuracies of surrogate models for CFE prediction				
Normalized generalized mean square cross validation errors (%)	12.9	19.7	17.5	**10.9**
Accuracies of surrogate models for SEA prediction				
Normalized generalized mean square cross validation errors (%)	17.9	25.4	22.5	**14.5**

where y_{max} and y_{min} are the maximum and minimum values of the response evaluated at the training points, respectively.

As noted earlier, the effects of the use of the lateral circular cutouts are evaluate by comparing the energy absorption capacity of the thin-walled tubes with lateral circular cutouts to those of the tubes without cutouts. Therefore, separate sets of surrogate models are constructed for the thin-walled tubes with and without cutouts.

Accuracies of surrogate models constructed for CFE and SEA predictions for the tubes without cutouts are given in Table 4. For the surrogate models constructed to predict CFE, the most accurate surrogate model is found to be the RBF model with 7.3% normalized *GMSE* value. For surrogate models constructed to predict SEA, however, the most accurate surrogate model is found to be the KR1 model with 5.5% normalized *GMSE* value. Both of these models have good levels of accuracy for a nonlinear crash problem.

Accuracies of surrogate models constructed for CFE and SEA predictions for the tubes with lateral circular cutouts are given in Table 5. The most accurate surrogate model type for prediction of both the CFE and the SEA is found to be the KR1 model. KR1 model for CFE prediction has 10.9% normalized *GMSE* value, and the KR1 model for SEA prediction has 14.5% normalized *GMSE* value. Both of these models have acceptable levels of accuracy for a nonlinear crash problem.

5.4. Surrogate-based optimization

Based on our earlier finding that the use of the most accurate surrogate model in optimization does not necessarily lead to the optimum solution [2], the optimizations of the tubes are performed with different surrogate model types, multiple optimum candidates are obtained, and the candidate with best performance (i.e., the smallest objective function) is chosen to be the optimum configuration. Finally, the surrogate model predictions at the optimum tube configurations are validated using LS-DYNA. Surrogate-based approach followed for optimization of the tubes is depicted in Fig. 10.

6. Optimization results

In this section, first the optimization results for the thin-walled tubes without cutouts are presented that provides a basis for comparison for the optimization results for the thin-walled tubes with cutouts. Then, the optimization results for the tubes with lateral circular cutouts are presented and discussed. Finally, FEA of the optimum designs are performed to validate the performances of optimum designs obtained through surrogate-based optimization approach.

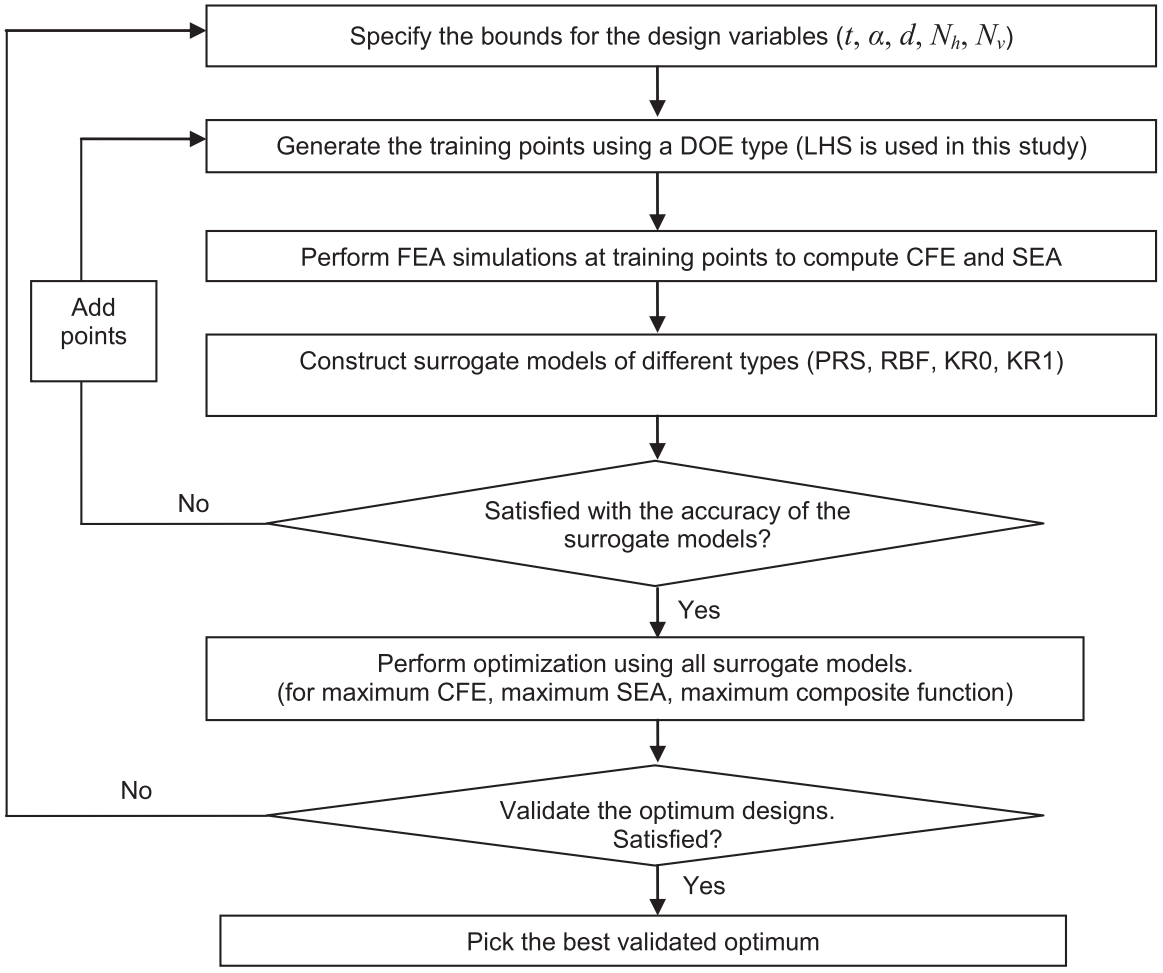

Fig. 10. Surrogate-based approach for optimization of the tubes.

Table 6
Optimization results for the tubes *without* cutouts for maximum CFE. *The maximum CFE value obtained via FEA is shown in bold font.*

Surrogate model	t (mm)	α (deg.)	CFE via surrogate	CFE via FEA
PRS	2.500	15.00	0.7336	0.6471
RBF	2.500	15.00	0.8439	0.6471
KR0	2.324	15.00	0.7335	0.6774
KR1	2.295	15.00	0.7154	**0.6812**

Table 7
Optimization results for the tubes *without* cutouts for maximum SEA. *The maximum SEA value obtained via FEA is shown in bold font.*

Surrogate model	t (mm)	α (deg.)	SEA via surrogate	SEA via FEA
PRS	2.500	15.00	22.68	19.96
RBF	2.500	15.00	24.40	19.96
KR0	2.500	2.12	22.70	**22.33**
KR1	2.500	0.00	22.05	21.49

6.1. Thin-walled tubes without cutouts

First, optimization of the tubes without cutouts is performed for maximum CFE using each surrogate model separately. Table 6 presents the optimum tube configurations, CFE predictions via surrogate models, and the CFE values computed via FEA. The optimum candidate designs obtained through PRS and RBF models are the same, whereas the other optimum candidate designs of the other surrogate models are slightly different. It is observed that all optimum candidates have the same taper angle of 15° (the upper bound). The last column of Table 6 shows that KR1 model provides the largest CFE (obtained via FEA) amongst the four optimum candidates, even though the globally most accurate surrogate model for CFE prediction is RBF (see Table 4). Note that the optimum CFE value (CFE=0.6812) is larger than the maximum CFE value obtained at the training points (CFE=0.6767, see Table 3). It is found that the optimal wall thickness is 2.295 mm and the optimal taper angle is 15° for maximum CFE. The optimum CFE value for the tubes without cutouts (CFE=0.6812) will be compared to the optimum CFE value of the tubes with lateral circular cutouts in Section 6.2 to evaluate the effect of introducing cutouts on CFE of the tubes.

Next, optimization of the tubes without cutouts for maximum SEA is performed. Table 7 lists the optimum tube configurations, SEA predictions via surrogate models, and the SEA values computed via FEA. Similar to the observation for the CFE optimization, the optimum candidate designs obtained through PRS and RBF models are the same, whereas the other optimum candidate designs are slightly different. It is observed that all optimum candidates have the same wall thickness value of 2.5 mm (the upper bound). The last column of Table 7 shows that KR0 model provides the largest SEA (obtained via FEA) amongst the four optimum candidates, even though the globally most accurate surrogate model for SEA prediction is KR1 (see Table 4). Note that the optimum SEA value (SEA=22.33) is larger than the maximum SEA value obtained at the training points (CFE=21.49, see Table 3). It is found that the optimal wall thickness is 2.5 mm and the optimal taper angle is around 2° for maximum SEA. Comparing the optimum tube configurations for maximum CFE and maximum SEA to each other, it is observed that the taper angle reaches its upper bound for maximum CFE and the wall thickness reaches its upper bound for maximum SEA. The optimum SEA value for the tubes without cutouts (SEA=22.33) will be compared to the optimum SEA value of the tubes with lateral circular cutouts in Section 6.2 to evaluate the effect of introducing cutouts on SEA of the tubes.

Finally, the tubes are optimized for the composite objective function (see Eq. (3)) that provides a compromise between the CFE and SEA. The case when CFE and SEA are equally important is considered, so the weight factor in Eq. (3) is taken as w=0.5. The values of CFE_0 and SEA_0 in Eq. (2) are taken as 0.6767 and 21.49, respectively. The optimization results are provided in Table 8. It is observed that the KR0 model yields the maximum composite objective function (F) value. The taper angle reaches to its upper bound, meaning that even though w=0.5 is used in Eq. (3) CFE dominates the behavior of F. Note also that the optimum F value (F=0.9446) is smaller than the maximum composite objective function value obtained at the training points (F=1, see Table 3).

Table 8
Optimization results for the tubes *without* cutouts for maximum F (composite objective function) with $w=0.5$. *The maximum F value obtained via FEA is shown in bold font.*

Surrogate model	t (mm)	α (deg.)	F via surrogate	F via FEA	CFE via FEA	SEA via FEA
PRS	2.500	15.00	1.070	0.9425	0.6471	19.96
RBF	2.500	15.00	1.191	0.9425	0.6471	19.96
KR0	2.348	15.00	1.068	**0.9446**	0.6698	19.33
KR1	2.500	15.00	1.021	0.9425	0.6471	19.96

Table 9
Optimization results for the tubes *with* lateral circular cutouts for maximum CFE. *The maximum CFE value obtained via FEA is shown in bold font.*

Surrogate model	t (mm)	α (deg.)	D	N_h	N_v	CFE via surrogate	CFE via FEA
PRS	3.500	15.00	5.00	2	5	0.9277	**0.8679**
RBF	3.500	15.00	5.00	2	1	0.9507	0.8659
KR0	3.257	13.67	9.50	4	2	0.7735	0.7198
KR1	3.500	14.35	9.22	4	1	0.7577	0.7710

6.2. Thin-walled tubes with lateral circular cutouts

First, optimization of the tubes with lateral circular cutouts is performed for maximum CFE using each surrogate model separately. Table 9 presents the optimum tube configurations, CFE predictions via surrogate models, and the CFE values computed via FEA. The optimum designs obtained through PRS and RBF models are the same, whereas the other optimum candidate designs are different. The last column of Table 9 shows that PRS model provides the largest CFE (obtained via FEA) amongst the four optimum candidates, even though the globally most accurate surrogate model for CFE prediction is KR1 (see Table 5). Note that the optimum CFE value (CFE=0.8679) is larger than the maximum CFE value obtained at the training points (CFE=0.7427). Note also that the optimum CFE value for the tubes with lateral circular cutouts (CFE=0.8679) is 27.4% larger than the optimum CFE value for the tubes without cutouts (CFE=0.6812).

It is found that the optimal wall thickness is 3.5 mm (the upper bound) and the optimal taper angle is 15° (the upper bound) for maximum CFE. The optimal cutout diameter is found to be 5 mm

Table 10
Optimization results for the tubes *with* lateral circular cutouts for maximum SEA. *The maximum SEA value obtained via FEA is shown in bold font.*

Surrogate model	t (mm)	α (deg.)	D	N_h	N_v	SEA via surrogate	SEA via FEA
PRS	3.500	15.00	5.00	2	5	32.72	26.14
RBF	3.500	0.00	5.00	2	1	36.58	26.26
KR0	3.411	6.53	9.22	5	4	27.21	**28.23**
KR1	3.500	0.00	5.00	2	5	27.79	23.53

Table 11
Optimization results for the tubes *with* lateral circular cutouts for maximum F (composite objective function) with $w=0.5$. *The maximum F value obtained via FEA is shown in bold font.*

Surrogate model	t (mm)	α (deg.)	D	N_h	N_v	F via surrogate	F via FEA	CFE via FEA	SEA via FEA
PRS	3.500	15.00	5.00	2	5	1.234	**1.071**	0.8679	26.14
RBF	3.500	0.00	5.00	2	1	1.205	0.827	0.5023	26.26
KR0	3.315	13.15	9.04	4	2	1.001	0.909	0.7017	23.41
KR1	3.500	15.00	5.00	2	5	1.007	**1.071**	0.8679	26.14

(the lower bound) for maximum CFE. The optimal number of cutouts in horizontal direction is found to be two (the lower bound), and the optimal number of cutouts in vertical direction is found to be five (the upper bound) for maximum CFE. That is, placing low number of cutouts in horizontal direction and high number of cutouts in vertical direction maximizes CFE.

Next, optimization of the tubes with lateral circular cutouts is performed for maximum SEA. Table 10 presents the optimum tube configurations, SEA predictions via surrogate models, and the SEA values computed via FEA. The optimum designs obtained through RBF and KR1 models are the same, whereas the other optimum candidate designs are different. The last column of Table 10 shows that KR0 model provides the largest SEA (obtained via FEA) amongst the four optimum candidates, even though the globally most accurate surrogate model for SEA prediction is KR1 (see Table 5). Note that the optimum SEA value (SEA=28.23) is larger than the maximum SEA value obtained at the training points (CFE=6.84). Note also that the optimum SEA value for the tubes with lateral circular cutouts (SEA=28.23) is 26.4% larger than the optimum SEA value for the tubes without cutouts (SEA=22.33).

It is found that the optimal wall thickness is 3.411 mm and the optimal taper angle is around 9° for maximum SEA. The optimal cutout diameter is found to be 9.22 mm for maximum SEA (recall that the cutout diameter reached its lower bound for maximum CFE). The optimal number of cutouts in horizontal direction is found to be five, and the optimal number of cutouts in vertical direction is found to be four for maximum SEA. It is observed for the optimum SEA design that the wall thickness is slightly reduced, the taper angle is significantly reduced, the cutout diameter is significantly increased, the number of cutouts in horizontal direction is increased, and the number of cutouts in vertical direction is slightly reduced compared to the optimum CFE design.

Finally, optimization of the tubes with lateral circular cutouts is performed for maximum composite objective function with w=0.5 (i.e., the case when CFE and SEA are equally important is considered). The values of CFE_0 and SEA_0 in Eq. (2) are taken as 0.7427 and 26.84, respectively. The optimization results are given in Table 11, which shows that the PRS and KR1 models result in the same optimum design and yield the maximum composite objective function (F) value. It is observed that the optimum design that maximizes F is the same design that maximizes CFE. That is, even though w=0.5 is used in composite objective function, CFE dominates the behavior of F. Note also that the optimum F value (F=1.071) is larger than the maximum composite objective function value obtained at the training points (F=0.981).

7. Conclusion

In this paper, the effects of introducing lateral circular cutouts on the crash performances of tapered thin-walled tubes were explored within a simulation-driven surrogate-based optimization approach. The specific energy absorption, SEA, and crush force efficiency, CFE, of the tubes were maximized using surrogate models. The design variables were selected as the wall thickness, the taper angle, the cutout diameter and the numbers of cutouts in horizontal and vertical directions In addition, multi-objective optimization of the tubes was performed by maximizing a composite objective function that provides a compromise between CFE and SEA. Based on the results obtained in this study, the following conclusions were drawn:

- The optimum CFE of the tubes with lateral circular cutouts was 27.4% larger than the optimum CFE of the tubes without cutouts.
- The optimum SEA of the tubes with lateral circular cutouts was 26.4% larger than the optimum SEA of the tubes without cutouts.
- Placing low number of cutouts in horizontal direction and high number of cutouts in vertical direction maximizes CFE.
- The optimum SEA design had slightly reduced wall thickness, significantly smaller taper angle, substantially larger cutout diameter, more cutouts in horizontal direction and less cutouts in vertical direction compared to the optimum CFE design.
- Multi-objective optimization based on the use of composite objective function that provides a compromise between CFE and SEA showed that the CFE dominates the behavior of composite objective function.
- For the tubes without cutouts, KR1 model provided the optimum CFE design even though the globally most accurate surrogate model for CFE prediction was RBF. Similarly, KR0 model provided the optimum SEA design, even though the globally most accurate surrogate model for SEA prediction was KR1.
- For the tubes with cutouts, PRS model provided the optimum CFE, even though the globally most accurate surrogate model for CFE prediction was KR1. Similarly, KR0 model provided the optimum SEA, even though the globally most accurate surrogate model for SEA prediction was KR1.
- The last two conclusions were in line with our earlier finding that the globally most accurate surrogate model does not necessarily lead to the optimum. Therefore, the best strategy in surrogate-based optimization approach is to construct as many surrogate models as possible, perform optimization by using these surrogate models to generate several candidates for optimum design, and finally, amongst the several candidates, the candidate that displays the best performance in terms of the responses of interest is selected as the optimum design.

Acknowledgments

This study is funded by The Scientific and Research Council of Turkey (TÜBİTAK) under Grant MAG-115M025.

References

[1] M.A. Guler, M.E. Cerit, B. Bayram, B. Gerçeker, E. Karakaya, The effect of geometrical parameters on the energy absorption characteristics of thin-walled structures under axial impact loading, Int. J. Crashworthiness 15 (2010) 377–390, http://dx.doi.org/10.1080/13588260903488750.
[2] E. Acar, M.A. Guler, B. Gereker, M.E. Cerit, B. Bayram, Multi-objective crashworthiness optimization of tapered thin-walled tubes with axisymmetric

indentations, Thin-Walled Struct. 49 (2011) 94–105, http://dx.doi.org/10.1016/j.tws.2010.08.010.
[3] M. Avalle, G. Chiandussi, Optimisation of a vehicle energy absorbing steel component with experimental validation, Int. J. Impact Eng. 34 (2007) 843–858, http://dx.doi.org/10.1016/j.ijimpeng.2006.02.001.
[4] S.S. Hsu, N. Jones, Quasi-static and dynamic axial crushing of thin-walled circular stainless steel, mild steel and aluminium alloy tubes, Int. J. Crashworthiness 9 (2004) 195–217, http://dx.doi.org/10.1533/ijcr.2004.0282.
[5] M. Langseth, O.S. Hopperstad, Static and dynamic axial crushing of square thin-walled aluminium extrusions, Int. J. Impact Eng. 18 (1996) 949–968, http://dx.doi.org/10.1016/S0734-743X(96)00025-5.
[6] S. Hou, Q. Li, S. Long, X. Yang, W. Li, Design optimization of regular hexagonal thin-walled columns with crashworthiness criteria, Finite Elem. Anal. Des. 43 (2007) 555–565, http://dx.doi.org/10.1016/j.finel.2006.12.008.
[7] H. Yin, G. Wen, S. Hou, K. Chen, Crushing analysis and multiobjective crashworthiness optimization of honeycomb-filled single and bitubular polygonal tubes, Mater. Des. 32 (2011) 4449–4460, http://dx.doi.org/10.1016/j.matdes.2011.03.060.
[8] S.R. Reid, T.Y. Reddy, Static and dynamic crushing of tapered sheet metal tubes of rectangular cross-section, Int. J. Mech. Sci. 28 (1986) 623–637, http://dx.doi.org/10.1016/0020-7403(86)90077-9.
[9] G.M. Nagel, D.P. Thambiratnam, Dynamic simulation and energy absorption of tapered tubes under impact loading, Int. J. Crashworthiness 9 (2004) 389–399, http://dx.doi.org/10.1533/ijcr.2004.0298.
[10] Y. Liu, Design optimisation of tapered thin-walled square tubes, Int. J. Crashworthiness 13 (2008) 543–550, http://dx.doi.org/10.1080/13588260802222102.
[11] S. Hosseinipour, G. Daneshi, Energy absorption and mean crushing load of thin-walled grooved tubes under axial compression, Thin-Walled Struct. 41 (2003) 31–46, http://dx.doi.org/10.1016/S0263-8231(02)00099-X.
[12] A.G. Mamalis, D.E. Manolakos, K.N. Spentzas, M.B. Ioannidis, S. Koutroubakis, P. K. Kostazos, The effect of the implementation of circular holes as crush initiators to the crushing characteristics of mild steel square tubes: experimental and numerical simulation, Int. J. Crashworthiness (2009), http://dx.doi.org/10.1080/13588260902826547.
[13] Q. Cheng, W. Altenhof, L. Li, Experimental investigations on the crush behaviour of AA6061-T6 aluminum square tubes with different types of through-hole discontinuities, Thin-Walled Struct. 44 (2006) 441–454, http://dx.doi.org/10.1016/j.tws.2006.03.017.
[14] S. Lee, C. Hahn, M. Rhee, J.-E. Oh, Effect of triggering on the energy absorption capacity of axially compressed aluminum tubes, Mater. Des. 20 (1999) 31–40, http://dx.doi.org/10.1016/S0261-3069(98)00043-0.
[15] A.A. Singace, H. El-Sobky, Behaviour of axially crushed corrugated tubes, Int. J. Mech. Sci. 39 (1997) 249–268, http://dx.doi.org/10.1016/S0020-7403(96)00022-7.
[16] A.M. Elgalai, E. Mahdi, A.M.S. Hamouda, B.S. Sahari, Crushing response of composite corrugated tubes to quasi-static axial loading, Compos. Struct. 66 (2004) 665–671, http://dx.doi.org/10.1016/j.compstruct.2004.06.002.
[17] S.B. Bodlani, S.C.K. Yuen, G.N. Nurick, The energy absorption characteristics of square mild steel tubes with multiple induced circular hole discontinuities—Part I: experiments, J. Appl. Mech. 76 (2009) 041012, http://dx.doi.org/10.1115/1.3114971.
[18] J. Song, Y. Chen, G. Lu, Light-weight thin-walled structures with patterned windows under axial crushing, Int. J. Mech. Sci. 66 (2013) 239–248, http://dx.doi.org/10.1016/j.ijmecsci.2012.11.014.
[19] B. Arnold, W. Altenhof, Experimental observations on the crush characteristics of AA6061 T4 and T6 structural square tubes with and without circular discontinuities, Int. J. Crashworthiness 9 (2004) 73–87, http://dx.doi.org/10.1533/ijcr.2004.0273.
[20] H. Han, F. Taheri, N. Pegg, Quasi-static and dynamic crushing behaviors of aluminum and steel tubes with a cutout, Thin-Walled Struct. 45 (2007) 283–300, http://dx.doi.org/10.1016/j.tws.2007.02.010.
[21] S.B. Bodlani, S.C.K. Yuen, G.N. Nurick, The energy absorption characteristics of square mild steel tubes with multiple induced circular hole discontinuities—Part II: numerical simulations, J. Appl. Mech. 76 (2009) 041012, http://dx.doi.org/10.1115/1.3114971.
[22] Livermore Software Technology Corporation, LS-DYNA Keyword User's Manual, vol. I, 2007.
[23] Euro-NCAP, EUROPEAN NEW CAR Assessment PROGRAMME (Euro NCAP) Frontal Impact, 2013, 52.
[24] J. Forsberg, L. Nilsson, Evaluation of response surface methodologies used in crashworthiness optimization, Int. J. Impact Eng. 32 (2006) 759–777, http://dx.doi.org/10.1016/j.ijimpeng.2005.01.007.
[25] J. Sobieszczanski-Sobieski, S. Kodiyalam, R.Y. Yang, Optimization of car body under constraints of noise, vibration, and harshness (NVH), and crash, Struct. Multidiscip. Optim. 22 (2001) 295–306, http://dx.doi.org/10.1007/s00158-001-0150-6.
[26] S. Kodiyalam, R.J. Yang, L. Gu, C.H. Tho, Multidisciplinary design optimization of a vehicle system in a scalable, high performance computing environment, Struct. Multidiscip. Optim. 26 (2004) 256–263 http://www.scopus.com/inward/record.url?eid=2-s2.0-1542712602&partnerID=tZOtx3y1.
[27] H. Kurtaran, A. Eskandarian, D. Marzougui, N.E. Bedewi, Crashworthiness design optimization using successive response surface approximations, Comput. Mech. 29 (2002) 409–421, http://dx.doi.org/10.1007/s00466-002-0351-x.
[28] M. Redhe, J. Forsberg, T. Jansson, P.O. Marklund, L. Nilsson, Using the response surface methodology and the D-optimality criterion in crashworthiness related problems, Struct. Multidiscip. Optim. 24 (2002) 185–194, http://dx.doi.org/10.1007/s00158-002-0228-9.
[29] H. Fang, M. Rais-Rohani, Z. Liu, M.F. Horstemeyer, A comparative study of metamodeling methods for multiobjective crashworthiness optimization, Comput. Struct. 83 (2005) 2121–2136, http://dx.doi.org/10.1016/j.compstruc.2005.02.025.
[30] T. Jansson, L. Nilsson, M. Redhe, Using surrogate models and response surfaces in structural optimization – With application to crashworthiness design and sheet metal forming, Struct. Multidiscip. Optim. 25 (2003) 129–140, http://dx.doi.org/10.1007/s00158-002-0279-y.
[31] S.-H. Lee, H.-Y. Kim, S.-I. Oh, Cylindrical tube optimization using response surface method based on stochastic process, J. Mater. Process. Technol. 130–131 (2002) 490–496, http://dx.doi.org/10.1016/S0924-0136(02)00794-X.
[32] Y. Xiang, Q. Wang, Z. Fan, H. Fang, Optimal crashworthiness design of a spot-welded thin-walled hat section, Finite Elem. Anal. Des. 42 (2006) 846–855, http://dx.doi.org/10.1016/j.finel.2006.01.001.
[33] K. Yamazaki, J. Han, Maximization of the crushing energy absorption of tubes, Struct. Optim. 16 (1998) 37–46, http://dx.doi.org/10.1007/BF01213998.
[34] L. Lanzi, L.M.L. Castelletti, M. Anghileri, Multi-objective optimisation of composite absorber shape under crashworthiness requirements, Compos. Struct. 65 (2004) 433–441, http://dx.doi.org/10.1016/j.compstruct.2003.12.005.
[35] H.R. Zarei, M. Kröger, Multiobjective crashworthiness optimization of circular aluminum tubes, Thin-Walled Struct. 44 (2006) 301–308, http://dx.doi.org/10.1016/j.tws.2006.03.010.
[36] S. Xie, H. Zhou, Analysis and optimisation of parameters influencing the out-of-plane energy absorption of an aluminium honeycomb, Thin-Walled Struct. 89 (2015) 169–177, http://dx.doi.org/10.1016/j.tws.2014.12.024.
[37] MATLAB User's Guide, MATH Work. Inc., 2009.
[38] HyperMesh 8.0 User's Guide, Altair Eng., 2006.
[39] G.G. Wang, S. Shan, Review of metamodeling techniques in support of engineering design optimization, J. Mech. Des. 129 (2007) 370–380.
[40] J.S. Park, Optimal Latin-hypercube designs for computer experiments, J. Stat. Plan. Inference 39 (1994) 95–111, http://dx.doi.org/10.1016/0378-3758(94)90115-5.
[41] C. Currin, T. Mitchell, M. Morris, D. Ylvisaker, Bayesian prediction of deterministic functions, with applications to the design and analysis of computer experiments, J. Am. Stat. Assoc. 86 (1991) 953–963 http://www.jstor.org/stable/2290511.
[42] M.E. Johnson, L.M. Moore, D. Ylvisaker, Minimax and maximin distance designs, J. Stat. Plan. Inference 26 (1990) 131–148, http://dx.doi.org/10.1016/0378-3758(90)90122-B.
[43] A.B. Owen, Orthogonal arrays for computer experiments, integration and visualization, Stat. Sin. 2 (1992) 439–452 http://apps.isiknowledge.com/InboundService.do?product=WOS&action=retrieve&SrcApp=Papers&UT=A1992JQ01200007&SID=Q2bLAlDeDMoNNjgB84J&SrcAuth=mekentosj&mode=FullRecord&customersID=mekentosj&DestFail=http://access.isiproducts.com/custom_images/wok_failed_aut.